Plasmon localization and local field distribution in metal-dielectric films

Dentcho A. Genov, Andrey K. Sarychev, and Vladimir M. Shalaev
School of Electrical and Computer Engineering, Purdue University, West Lafayette, Indiana 47907-1285
(Received 12 October 2002; published 15 May 2003)

An exact and very efficient numerical method for calculating the effective conductivity and local-field distributions in random *R-L-C* networks is developed. Using this method, the local-field properties of random metal-dielectric films are investigated in a wide spectral range and for a variety of metal concentrations *p*. It is shown that for metal concentrations close to the percolation threshold ($p=p_c$) and frequencies close to the resonance, the local-field intensity is characterized by a non-Gaussian, exponentially broad distribution. For low and high metal concentrations a scaling region is formed that is due to the increasing number of noninteracting dipoles. The local electric fields are studied in terms of characteristic length parameters. The roles of both localized and extended eigenmodes in Kirchhoff's Hamiltonian are investigated.

DOI: 10.1103/PhysRevE.67.056611 PACS number(s): 78.68.+m, 78.67.−n, 78.20.−e, 73.61.−r

I. INTRODUCTION

The last two decades were a time of immense improvement in our understanding of the optical properties of inhomogeneous media [1]. One of the important representatives of such media is a metal-dielectric composite near the percolation threshold. Such nanostructured composite materials are of significant interest because they can lead to dramatic enhancement of optical responses in a broad spectral range, including the visible and infrared parts of the spectrum. In particular, percolation metal-dielectric films can be employed for surface-enhanced spectroscopy with unsurpassed sensitivity and for developing optical elements, such as optical switches and efficient optical filters, with transparency windows that can be induced by local photomodification in the composite films.

In the optical and infrared spectral ranges, the metal dielectric permittivity has, typically, a negative real part, so that metal particles can be viewed as inductance elements with small losses (*R-L* elements). In accordance with this assumption, a metal-dielectric composite can be treated as an *R-L-C* network, where the *C* elements stand for dielectric grains, which have a positive dielectric permittivity. Many different approaches based on effective-medium theories and various numerical models have been suggested to describe the optical nonlinearities of such systems [2]. In particular, a number of numerical simulations have been carried out by using the real space renormalization group [3–8]. A recently developed scaling theory [4–8] for the field fluctuations and high-order field moments predicts localization of the surface plasmons in percolation composites and strong enhancement for the local field, resulting from the localization. Experimental observations [7,9] in accord with the theoretical predictions show the existence of giant local fields, which can be enhanced by a factor of 10^5 for the linear response and 10^{20} and greater for the nonlinear response. A recent study [10] of the plasmon modes in metal-dielectric films gives more insights into the problem. Thus, in Ref. [10] it was found that for all systems studied the local fields are concentrated in nanometer sized areas, while some of the eigenstates are not localized.

Despite the progress, computer modeling of the electric field distribution in metal-dielectric nanocomposites has been restricted so far to mainly approximate methods, such as the real space renormalization group (RSRG). To some extent, this was justified since the focus of those calculations was on the effective properties, such as the macroscopic conductivity and dielectric permittivity. Many fast algorithms were suggested for determining the effective conductivities; these include very efficient models, such as the Frank and Lobb Y-∇ transformation [11], the exact numerical renormalization in a vicinity of the percolation threshold [12–14], and the transfer matrix method [15]. Unfortunately, none of these methods can be used for precise calculation of the local-field distribution and a different approach is needed. The relaxation method (RM) was one of the first algorithms to give some insight into the field distributions [16]. This method has the advantage of using the minimum possible memory, which is proportional to the number of sites L^d, where L is the size of the system and d is the space dimensionality. Fast Fourier acceleration [17] allows one to speed up the convergency of the iteration process for both two- (2D) and three-dimensional (3D) percolation systems. However, the ''critical slowing down'' effect and the problem of stability (occurring when the imaginary part of the local conductivity takes both positive and negative values) restrict the use of this approach. Thus, the local-field statistics for percolation composites in the optical and infrared spectral ranges was not investigated until very recently, with direct numerical methods that do not involve any *a priori* assumptions. In their work, Zekri, Bouamrane, and Zekri [18] suggested a substitution method, which allows one to calculate the local-field distributions in percolation metal-dielectric composites in the optical range. However, results obtained for the local-field intensity distribution function $P(I)$ (where $I=|E|^2$) appear to be rather surprising. Specifically, instead of the theoretically predicted and experimentally observed enhancement for the local field, the authors of Ref. [18] obtained strong dissipation, so that the average field intensity was even lower than the applied one. This contradiction with the previous results for the local-field distribution and the necessity for a more accurate method was one of the motivations for this work. We note that the high local fields play a crucial role in enhancement for nonlinear optical effects

and thus it is important to verify this prediction by exact calculations.

In this paper we suggest a direct numerical method, which we refer to as block elimination (BE). The BE method allows calculations of effective parameters (such as the conductivity, dielectric permittivity, etc.) and, most importantly, the local-field distribution in inhomogeneous media. In this work we focus our attention on the local-field distribution $P(I)$ and compare results obtained by BE with those following from the RSRG, the relaxation method, and the Zekri-Bouamrane-Zekri (ZBZ) method. Specifically, we investigate the properties of two-dimensional random metal-dielectric composites by modeling them as a square lattice with the lattice size L comprised of dielectric and metal bonds, with conductivities σ_d and σ_m, respectively. The probability of a bond to have metallic conductivity is p (where p is the metal concentration) and the probability of dielectric conductivity is $1-p$. In agreement with earlier theoretical predictions and experimental observations [4–9], we obtain a ''topology'' of the local electric field characterized by sharp peaks that can exceed the applied field by several orders of magnitude. The field maxima are due to the effect of localization of the surface plasmon modes in random films [7]. A full set of field distribution functions $P(I)$ that gradually transform from ''one-dipole'' field distribution to log-normal distribution are calculated by using the BE method.

The rest of this paper is organized as follows. In Sec. II, we describe the block elimination procedure and some basic equations describing metal-dielectric composites. In Sec. III, we examine the accuracy of this method by calculating the critical behavior and the effective conductivities for some important cases. In Sec. IV, we study the local-field distribution $P(I)$ for different metal concentrations p and conductivities σ_m. In Sec. V, using an approach based on the inverse participation ratio, we find important relations for the field correlation length ξ_e, average field localization length ξ_f, and average distance between metal particles ξ_a. The eigenvalue problem is solved here and effects due to the existence of extended states are investigated. Finally, in Sec. VI we discuss the results obtained and draw conclusions.

II. BLOCK ELIMINATION METHOD

We consider the problem of a local-field distribution in nanoscale metal-dielectric films at and away from the percolation threshold, in the case when the wavelength λ of an incident light is much larger than the metal grain size a. Under this condition, we can introduce the local potential $\varphi(\mathbf{r})$ and local current $\mathbf{j}(\mathbf{r})=\sigma(\mathbf{r})\cdot[-\nabla\varphi(\mathbf{r})+\mathbf{E}_0]$, where $\mathbf{E}_0$ is the applied field and $\sigma(\mathbf{r})$ is the local conductivity. In the quasistatic case considered, the problem of the potential distribution is reduced to the solution of the current conservation law $\nabla\cdot\mathbf{j}(\mathbf{r})=0$, which leads to the Laplace equation $\nabla\cdot\{\boldsymbol{\sigma}(\mathbf{r})\cdot[-\nabla\varphi(\mathbf{r})+\mathbf{E}_0]\}=0$ for determining the potentials. Now we discretize the above relation on a square lattice so that the film, which is a binary composite of metal and dielectric particles, can be represented through metal and dielectric bonds connecting the lattice sites. Under such discretization the current conservation for lattice site i acquires the following form:

$$\sum_j \sigma_{ij}(\varphi_i-\varphi_j+E_{ij})=0, \tag{1}$$

where φ_i is the field potential of site i. The summation is over the nearest (to i) neighbor sites j; $\sigma_{ij}=\sigma_{ji}$ are the conductivities of bonds that connect neighbor sites i and j and E_{ij} are the electromotive forces. The electromotive forces E_{ij} are defined so that $E_{ij}=aE_0$, for the bond leaving site i in the $+y$ direction, and $E_{ij}=-aE_0$, for the bond in the $-y$ direction; E_{ij} is zero for the x bonds. Note that $E_{ij}=-E_{ji}$.

Numerical solutions of the Kirchhoff equation (1) in the case of large lattice sizes encounter immense difficulties and require very large memory storage and high operational speed. A full set of the Kirchhoff equations for a square lattice with size L is comprised of L^2 separate equations. This system of equations can be written in the matrix form

$$\hat{\mathbf{H}}\cdot\boldsymbol{\Phi}=\mathbf{F}, \tag{2}$$

where $\hat{\mathbf{H}}$ is a symmetric $L^2\times L^2$ matrix that depends on the structure and composition of the lattice, $\boldsymbol{\Phi}=\{\varphi_i\}$, and $\mathbf{F}=\{-\Sigma_j\sigma_{ij}E_{ij}\}$ are vectors of size L^2, which represent the potential and applied field at each site and bond. In the literature, the matrix $\hat{\mathbf{H}}$ is called the Kirchhoff Hamiltonian (KH) and it is shown to be similar to the Hamiltonian for the Anderson transition problem in quantum mechanics [5,7–9]. The Kirchhoff Hamiltonian is a sparse random matrix with diagonal elements $H_{ii}=\Sigma_j\sigma_{ij}$ (where the summation is over all bond conductivities σ_{ij} that connect the ith site with its neighbors) and nonzero off-diagonal elements $H_{ij}=-\sigma_{ij}$. For a detailed description of the KH, see the Appendix.

In principle, Eq. (2) can be solved directly by applying the standard Gaussian elimination to the matrix $\hat{\mathbf{H}}$ [19]. This procedure has a run time proportional to $\sim L^6$ and requires a memory space of the order of L^4. Simple estimations show that direct Gaussian elimination cannot be applied for large lattice sizes, $L>40$, because of the memory restrictions and long run times for all contemporary personal computers. Fortunately, the KH matrix $\hat{\mathbf{H}}$ has a simple symmetrical structure that allows implementation of the block elimination procedure which can significantly reduce the operational time and memory.

In calculations, we can apply the periodic boundary conditions for the x and y directions; alternatively, we can also impose parallel or L-electrode-type boundaries. In the case of the periodic boundary conditions, we suppose that the sites in the first row of the $L\times L$ lattice are connected to the Lth row, whereas the sites of the first column are connected to the last column. Then the Kirchhoff equations for the first site in the first row, for example, have the following form:

$$\sigma_{1,L}(\varphi_1-\varphi_L)+\sigma_{1,2}(\varphi_1-\varphi_2)+\sigma_{1,L^2-L+1}(\varphi_1-\varphi_{L^2-L+1}-aE_0)+\sigma_{1,L+1}(\varphi_1-\varphi_{L+1}+aE_0)=0, \tag{3}$$

where $\sigma_{1,L}$ is the conductivity of the bond connecting the first and the last sites in the first row. The $\sigma_{1,2}$ conductivity connects the first and second sites in the first row, σ_{1,L^2-L+1} connects the first site of the first row and the first site of the Lth row, $\sigma_{1,L+1}$ connects the first sites of the first and the second rows, and the external field E_0 is applied in the $+y$ direction. Note that the $\sigma_{1,L}$ and σ_{1,L^2-L+1} connections are due to the periodic boundary conditions in the x and y directions, respectively.

In Eq. (3) we numerate the sites of the $L\times L$ lattice "row by row," from 1 (for the first site in the first row) to L^2 (for the last site in the Lth row). Under this labeling the KH matrix $\hat{\mathbf{H}}$ acquires a block-type structure. As an example, for a system with size $L=5$, the matrix $\hat{\mathbf{H}}$ takes the following block form:

$$\hat{\mathbf{H}}=\begin{pmatrix} h^{(11)} & h^{(12)} & 0 & 0 & h^{(15)} \\ h^{(21)} & h^{(22)} & h^{(23)} & 0 & 0 \\ 0 & h^{(32)} & h^{(33)} & h^{(34)} & 0 \\ 0 & 0 & h^{(43)} & h^{(44)} & h^{(45)} \\ h^{(51)} & 0 & 0 & h^{(54)} & h^{(55)} \end{pmatrix}, \tag{4}$$

where $h^{(jj)}$ are $L\times L$ matrices with diagonal elements $h_{ii}^{(jj)}=\Sigma_k \sigma_{i+(j-1)L,k}$ [the summation is over the nearest neighbors of the site $i+(j-1)L$, which are located in the jth row, $1\leqslant i\leqslant L$], while the diagonal matrices $h^{(kl)}=h^{(lk)}(k\neq l)$ connect the kth row with the lth row, and vice versa. The matrices in the right upper and in the left bottom corners of the KH matrix $\hat{\mathbf{H}}$ are due to the periodical boundary conditions: they connect the top and the bottom rows and the first and the last columns. The explicit forms for the matrices $h^{(jj)}$ and $h^{(kl)}$ are given in the Appendix.

For large sizes L, the majority of the block $h^{(ij)}$ are zero matrices and applying Gaussian elimination will be a very inefficient way to solve the system Eq. (2). In fact, in a process of elimination of all block elements below $h^{(11)}$ in the matrix Eq. (4), the only matrix elements that will change are $h^{(11)}$, $h^{(12)}$, $h^{(22)}$, $h^{(15)}$, and $h^{(55)}$, with two more elements appearing in the second and last rows. Thus, to eliminate the first block column of the KH we can instead of $\hat{\mathbf{H}}$ work with the following $3L\times 3L$ block matrix:

$$\hat{\mathbf{h}}^{(1)}=\begin{pmatrix} h^{(11)} & h^{(12)} & h^{(15)} \\ h^{(21)} & h^{(22)} & 0 \\ h^{(51)} & 0 & h^{(55)} \end{pmatrix}, \tag{5}$$

recall that in the considered example we choose, for simplicity, $L=5$.

Now to eliminate all elements below the diagonal in the first block column of matrix $\hat{\mathbf{h}}^{(1)}$ we apply a standard procedure [19], whereby, using the diagonal elements of block matrix $h^{(11)}$ as pivots, we transform $h^{(11)}$ into a triangle matrix $h^{*(11)}$ and simultaneously eliminate $h^{(21)}$ and $h^{(51)}$. The elimination of the first column of $\hat{\mathbf{h}}^{(1)}$and correspondingly $\hat{\mathbf{H}}$ thus requires only L^3 simple arithmetical operations which is to be compared with L^5 operations needed if we work directly with the whole matrix $\hat{\mathbf{H}}$. After the first step of this block elimination is completed the matrix $\hat{\mathbf{H}}$ has the following form:

$$\hat{\mathbf{H}}^{(1)}=\begin{pmatrix} h^{*(11)} & h^{*(12)} & 0 & 0 & h^{*(15)} \\ 0 & h^{*(22)} & h^{(23)} & 0 & h^{(25)} \\ 0 & h^{(32)} & h^{(33)} & h^{(34)} & 0 \\ 0 & 0 & h^{(43)} & h^{(44)} & h^{(45)} \\ 0 & h^{(52)} & 0 & h^{(54)} & h^{*(55)} \end{pmatrix}, \tag{6}$$

where by the asterisk superscript we denote all blocks that have changed in the elimination process. The two new block elements $h^{(25)}$ and $h^{(52)}$ appeared due to the interactions of the first row with the second and the fifth rows.

As a second step, we apply the above procedure for the minor $\hat{\mathbf{H}}_{11}^{(1)}$ of the matrix $\hat{\mathbf{H}}^{(1)}$ (which now plays the role of $\hat{\mathbf{H}}$); therefore we work again with a $3L\times 3L$ matrix:

$$\hat{\mathbf{h}}^{(2)}=\begin{pmatrix} h^{*(22)} & h^{(23)} & h^{(25)} \\ h^{(32)} & h^{(33)} & 0 \\ h^{(52)} & 0 & h^{*(55)} \end{pmatrix}. \tag{7}$$

Repeating with $\hat{\mathbf{h}}^{(2)}$ all operations we performed on $\hat{\mathbf{h}}^{(1)}$, we put $h^{*(22)}$ in the triangle form and eliminate $h^{(32)}$ and $h^{(52)}$. We continue this procedure until the whole matrix $\hat{\mathbf{H}}$ is converted into the triangular form with all elements below the diagonal being zero. The backward substitution for a triangular matrix is straightforward; namely, we obtain first the site potentials in the Lth row (the fifth row, in our example) and then, by calculating the potentials, in the $(L-1)$th row, and so on, until the potentials in all rows are obtained. The total number of operations needed is estimated as $\sim L^4$, for the described block elimination method, which is less than the number L^6 needed for Gaussian or **LU** (for symmetric matrixes) elimination [19]. The BE has operational speed of the same order of magnitude as in the transfer-matrix method [15] and the Zekri-Bouamrane-Zekri method [18]. However, BE allows the calculation of the local fields, as opposed to the Frank-Lobb method, and we believe that it is much easier in numerical coding when compared to the ZBZ method.

For each step of the BE procedure, we need to keep only L^2 (the matrix $\hat{\mathbf{h}}^{(k)}$) complex numbers in the operational memory and L^3 on a hard disk. By using the hard drive we do not significantly decrease the speed performance because only L loadings of L^2 numbers are required, i.e., L^3 additional operations in total. Note that the BE, like to the Gaussian elimination, is well suited for parallel computing.

We performed various tests to check the accuracy of the BE algorithm described above. First, the sum of the currents in each site was calculated and the average value $\sim 10^{-14}$ was found; this is low enough to claim that current conservation holds in the method. Our calculations, using the standard Gaussian elimination (for small lattice sizes) and the relaxation method (for the case of all positive conductivi-

ties), for the effective conductivity and the local-field distribution show full agreement with results obtained using the block elimination procedure developed.

III. RESULTS FOR 2D PARALLEL AND *L*-TYPE LATTICES

In inhomogeneous media, such as metal-dielectric composites, both the dielectric permittivity $\varepsilon(\mathbf{r})$ and conductivity $\sigma(\mathbf{r})=-i\omega\varepsilon(\mathbf{r})/4\pi$ depend on the position $\mathbf{r}$. When the size of the composite is much larger than the size of inhomogeneities, the effective conductivity σ_e can be introduced. As discussed above, we model the composite by an *R-L-C* square lattice and then apply the BE method to find the field potentials in all sites of the lattice. When the potential distribution is known we can calculate the effective conductivity:

$$\sigma_e|\mathbf{E}_0|^2=\frac{1}{S}\int \sigma(\mathbf{r})|\mathbf{E}(\mathbf{r})|^2 d\mathbf{r}, \tag{8}$$

where $\mathbf{E}(\mathbf{r})$ and $\mathbf{E}_0$ are the local and applied fields, respectively (see, e.g., [2]).

It is well known that the effective dc conductivity for a two-component random mixture ($\sigma_m \gg \sigma_d$) should vanish as a power law, when the metal concentration p approaches the percolation threshold p_c, i.e.,

$$\sigma_e \sim \sigma_m (p-p_c)^t, \tag{9}$$

where t is the critical exponent, which has been calculated and measured by many authors. In the 2D case, the critical exponent is given by $t=1.28\pm0.03$, according to Derrida and Vannimenus [15], and $t=1.29\pm0.02$, according to Frank and Lobb [11]. The value $t=1.33\pm0.03$ was found by Sarychev and Vinogradov [13], who used the exact renormalization group procedure and reached the lattice size $L=500$ in their simulations. In all cases, the critical exponent t was calculated using finite-size scaling theory [20]. When the volume fraction p of the conducting elements reaches the percolation threshold p_c, the correlation length increases as $\xi \sim (p-p_c)^{-\nu}$, where $\nu=4/3$ is the critical exponent for the correlation length [2]. Because the correlation length ξ determines the minimum size of the network, for which it can be viewed as homogeneous, one expects that for $L \ll \xi$ the effective conductivity depends on the system size L. The finite-size scaling theory [20–23] predicts the following dependence:

$$\sigma_e(L) \sim L^{-t/\nu} f(\eta), \tag{10}$$

where the argument $\eta=L^{1/\nu}(p-p_c)$ depends on the system size L and on the proximity to the percolation threshold p_c. For a self-dual lattice, such as the square lattice considered here, the percolation threshold is known exactly: $p_c=0.5$. When calculations are carried out for $p=p_c$ there is no need for knowledge of the specific form of the function f in Eq. (10).

We calculate the effective conductivity $\sigma_e(L)$ for different sizes L. In order to improve the statistics for each size L, a number of distinct realizations were performed. Specifically we used 40 000 realizations for $L=10$; 5000 realizations for $L=20$; 1000 realizations for $L=60$; and 100 realizations for $L=150$. The data from our calculations were fitted to Eq. (10) and χ^2 analysis was applied to determine the critical exponents. Thus we found that $t/\nu=0.96\pm0.03$ and $t=1.28\pm0.04$. This result is in good agreement with the estimates of Derrida and Vannimenus and Frank and Lobb, but somewhat lower than the $t/\nu=1.0$ obtained by Sarychev and Vinogradov. Note that the value $t/\nu=1.0$ is expected for sizes $L>300$ that are greater than those we used in our estimates.

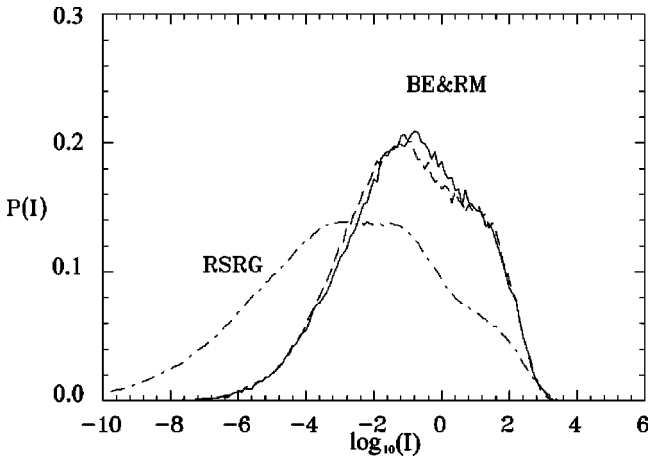

FIG. 1. The local-field distribution $P(I)$ calculated with two exact methods, the relaxation method (RM) and block elimination (BE). Results of calculations with the approximate, real space renormalization group (RSRG) are also shown. The ratio of the (real) conductivities for metal and dielectric bonds is chosen as $\sigma_m/\sigma_d=10^3$.

IV. LOCAL-FIELD DISTRIBUTION FUNCTION

To further verify the accuracy of the block elimination method, we explicitly tested the field distribution function, for the case when the conductivities are positive and real numbers (i.e., the dielectric permittivity is purely imaginary in this case). The local-field distribution function (LFDF) we sampled in terms of $\log_{10}(I)$, where $I=(|\mathbf{E}-\mathbf{E}_0|/|\mathbf{E}_0|)^2$ is the local-field intensity fluctuation with $|\mathbf{E}_0|^2$ being the intensity of the applied field. If the bond conductivities σ_d and σ_m are positive, we can also apply the relaxation method [17] and compare the results with those obtained with the BE procedure. Such a comparison is presented in Fig. 1, where we can see that both distributions are nearly the same, with only minor deviations due to the differences in the calculation procedures resulting in different round-off errors, and also due to nonsufficient relaxation times. In the same figure, the local-field distribution obtained with the real space renormalization group method is also shown. It exhibits an extended tail toward small values of the intensity I, a fact that is observed for all distributions calculated with this method.

Although the case of real positive values for the conductivities is of considerable interest, more important physical problems arises when the metal conductivity is complex. One special case corresponds to the surface plasmon reso-

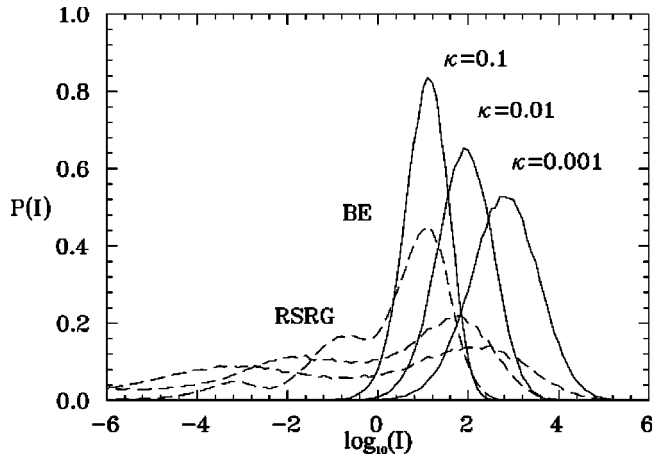

FIG. 2. Local-field distributions $P(I)$ calculated for three different loss factors $\kappa=0.1$, 0.01, and 0.001, using the BE and RSRG methods. All distributions are obtained for $p=p_c$.

nance, which plays a crucial role in the optical and infrared spectral ranges for metal-dielectric composites. For the two-dimensional case, this resonance for individual particles occurs when $\sigma_d \approx -\sigma_m$, and it can be investigated using a dimensionless set of conductivities $\sigma_d=-i$ and $\sigma_m=i+\kappa$, where i is the imaginary unit and κ is a small real "conductivity" that corresponds to the losses in the system. Recall that in metal-dielectric films the conductivity $\sigma_m=-i\omega\varepsilon_m/4\pi$ is predominantly imaginary with a very small real part [22]. In Fig. 2, we show the local-field distributions calculated for three different values of κ, using both the block elimination and the real space renormalization group procedures. All functions obtained by these two methods differ in shape and peak positions; however, taking into account that the RSRG is indeed an approximate procedure, we can conclude that qualitatively it performs rather well for high intensities. It is important to note that the local-field distribution is non-Gaussian and has a form close to the log-normal function:

$$P(I)=\frac{1}{\Delta I\sqrt{2\pi}}\exp\left[-\frac{[\log_{10}(I)-\langle\log_{10}(I)\rangle]^2}{2\Delta^2}\right], \quad (11)$$

where $\langle\log_{10}(I)\rangle$ is the average value for the logarithm of the local field intensity I and Δ is the standard deviation in terms of $\log_{10}(I)$. This approximation for the field distribution seems to work sufficiently well around the average value $\bar{s}=\langle\log_{10}(I)\rangle$. We note, however, that according to Ref. [24], where the current distribution was studied, Eq. (11) probably will fail for intensities I far from the logarithmic average $\bar{s}$. In Fig. 2 we can also see that $\langle\log_{10}(I)\rangle$ and Δ both increase when κ decreases.

Distributions similar in shape to those shown in Fig. 2 were obtained by Zekri *et al.*, and discussed in [18,25]. It was found that all distributions were shifted significantly toward smaller values of I, which led the authors to the conclusion that there is no strong enhancement for the local field. Such a conclusion contradicts earlier calculations [4–6,8], experimental observations [7,9], and the current

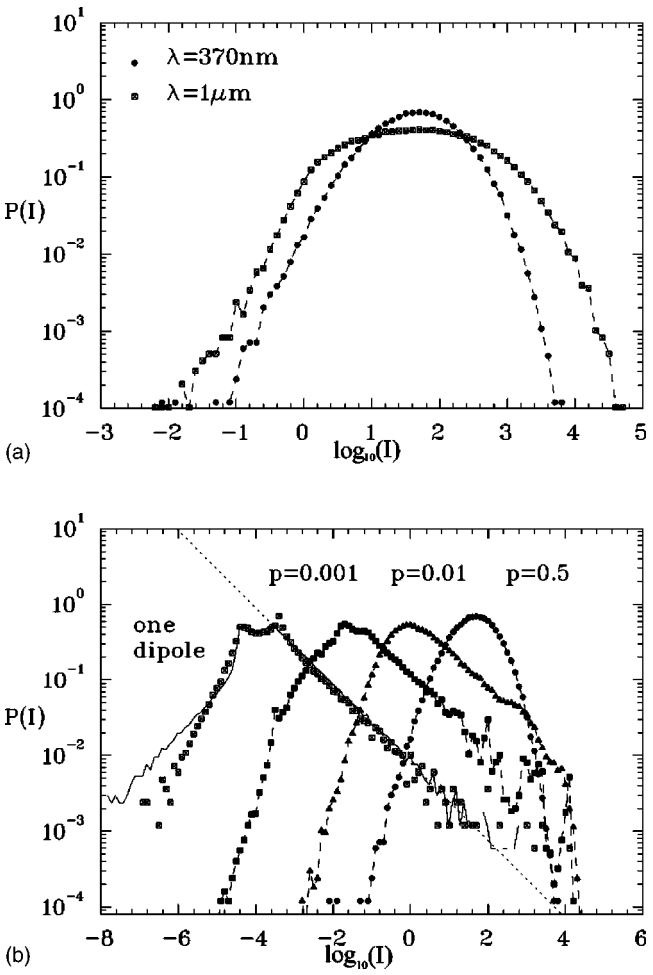

FIG. 3. Local-field distributions $P(I)$ for silver-glass films: (a) for $\lambda=370$ nm and $\lambda=1$ μm at $p=p_c$; (b) for different metal filling factors p at $\lambda=370$ nm; the dashed line corresponds to the analytically predicted single dipole distribution.

simulations based on the exact BE method. All these simulations and experiments indicate the existence of large local-field enhancement in percolation metal-dielectric films resulting from plasmon resonances.

In addition to the reference system with $\sigma_d=-i$ and $\sigma_m=i+\kappa$, we also did LFDF calculations for a silver-on-glass film using the Drude formula for the metal permittivity ε_m, given as

$$\varepsilon_m(\omega)=\varepsilon_b-(\omega_p/\omega)^2/(1+i\omega_\tau/\omega), \quad (12)$$

where ε_b is the contribution due to the interband transitions, ω_p is the plasma frequency, and $\omega_\tau=1/\tau\ll\omega_p$ is the relaxation rate. For silver, we used the following constants: $\varepsilon_b=5.0$, $\omega_p=9.1$ eV, and $\omega_\tau=0.021$ eV [26]; for the glass substrate, we used $\varepsilon_d=2.2$.

In Fig. 3(a) we show the local-field distribution for two different wavelengths: one corresponding to the resonance of individual particles $\omega=\omega_r$, occurring at $\sigma_d\approx-\sigma_m$ ($\lambda\sim370$ nm) and another in the infrared part of the spectrum. Again, we observe very wide distributions whose width increases with the wavelength and enhancement factors that

reach values of the order of $\sim 10^5$. We note that the log-normal approximation Eq. (11) does not hold for frequencies shifted away from the resonance. Changes in the shape of the LFDF are also observed when the surface metal coverage deviates from the percolation threshold value. This effect is shown in Fig. 3(b) where we have plotted the field distribution for three different metal concentrations $p=0.5$, 0.01, and 0.001 at the resonance $\lambda=370$ nm. The case of a single metal bond (dipole) positioned at the center of the film is also included. There is an apparent transition from the log-normal (for $p=p_c$) LFDF into distributions that have ''scaling'' power-law regions. The appearance of the scaling regions is due to a change in the composite, transforming from a strongly coupled dipole system at the percolation threshold into a randomly distributed, sparse configuration of noninteracting dipoles for lower metal concentrations. In two dimensions, a single dipole placed at the center of the coordinate system induces an electric field with intensity $I_{dip}(r,\theta)=\gamma\cos^2\theta/r^4$, where $r=|\mathbf{r}|$ is the modulus of the radius vector $\mathbf{r}=\{x,y\}$ and θ is the angle between the field polarization and $\mathbf{r}$. To find the actual one-dipole field distribution $P_{dip}(I)$ we consider the one-dipole intensity $I_{dip}(r,\theta)$ over the square lattice and then we count the ''identical'' magnitudes in the logarithm of the field-intensity I. The resultant curve for the one-dipole field distribution [the solid line in Fig. 3(b)] should be compared with the field distribution obtained from the Kirchhoff equations when there is only one metal bond in the center of the film. Both distributions match extremely well; it can be seen that our method captures even the smallest effects in the distribution caused by the cosine term. A fit for the scaling region, $P_{dip}(I)\sim I^{-\alpha}$, gives the same exponent $\alpha=3/2$ for different p. Such universal scaling was also obtained for fractals [27], where the scaling index α was found to be close to 1.5 and explained by the vector nature of the dipole fields. The same number for α can be obtained through the integral $P_{dip}(I)=\int\int\delta(I-I_{dip}(r))dS$, where $I_{dip}(r)\sim 1/r^4$, δ is the Dirac delta function and S represents the surface for integration. It is important to mention that the field distribution was obtained experimentally by direct measurements of the local field intensities [28,29]. It was found that LFDF is an exponential function with maximum field enhancement of the order of ~ 50. This strong decrease of the local-field intensity and the exponential shape of the distribution is explained by the destructive interference which occurs when the field is collected from large (compared to the particle sizes) areas [29]. When this effect is incorporated into a theoretical consideration, good agreement with experiment data is observed [29].

V. LOCALIZATION AND HIGH-ORDER FIELD MOMENTS

One of the most important properties of metal-dielectric composites is the localization of the surface plasmons. In Ref. [25], the authors performed estimations for surface plasmon localization, using the inverse participation ratio $R_{IP}=(\Sigma_i^N|\mathbf{E}_i-\mathbf{E}_0|^4)/(\Sigma_i^N|\mathbf{E}_i-\mathbf{E}_0|^2)^2=N^{-1}\langle I^2\rangle/\langle I\rangle^2$ [30], where $N=L^d$ is the total number of sites and $\mathbf{E}_i$ is the electric field vector corresponding to the ith site. According to Ref. [25], R_{IP} for extended plasmons should be size dependent and characterized by a scale comparable to the size of the system; if there is a tendency to localization, the corresponding exponent should decrease and, for strongly localized fields, it should become zero. For various loss factors κ the authors of [25] found that $R_{IP}\sim L^{-1.3}$ so that the field moment ratio is $R=\langle I^2\rangle/\langle I\rangle^2=R_{IP}\times L^d\sim L^{0.7}$. This result leads to size-dependent field moments, which for large L should not be the case. Below we show that the earlier theory [4–8], which is based on Eq. (1), is indeed size independent and we will support the conclusion on plasmon localization with the exact BE method. By investigating the scaling behavior of R we will also extract some important relationships that describe the statistical properties of the local fields in semicontinuous metal films.

We first focus on the simplest case when there is only one dipole in the entire space. For a single dipole it is easy to obtain the relation $R=\langle I^2\rangle/\langle I\rangle^2\simeq\frac{1}{3}\varkappa^{1/2}$, where $\varkappa=I_{max}/I_{min}$ is the ratio of the maximum (which is close to the dipole site) and minimum (away from the dipole) in the field intensities. Because of the power-law dependence $I_{dip}\sim r^{-4}$, there is a size dependence $R\simeq\frac{1}{3}(l/a)^2=\frac{1}{3}L^2$, where l is the length scale of the space that is under consideration and a is the average particle size. The function $R(L)$ as calculated for a single dipole in the center of the square mesh is shown in Fig. 4(a). The size dependence for the one-dipole local-field moments is an expected result since with an increase of the investigated volume the weight of the low-magnitude fields becomes progressively larger. However, for practical applications, we are interested in systems with large numbers of particles so that they can be viewed as macroscopically homogeneous. We can write this condition as $n_a=(l/\xi_a)^d\gg 1$, or $(aL/\xi_a)^d=pL^d\gg 1$, where p is the volume fraction and ξ_a is the average distance between the metal particles. Now for a theory to be size independent [$R(L)\sim$const] we must impose the homogeneity condition $L\gg p^{-1/d}$. In Fig. 4(a) we show $R(L)$ corresponding to the resonance case $\sigma_d=-i$ and $\sigma_m=i+\kappa$, with loss factor $\kappa=0.01$ and three different metal coverages $p=0.5$, 0.1, and 0.01. It is clearly seen that in the limit $L\gg p^{-1/d}$ there is an apparent transition from a size-dependent into a size-independent ratio R, as expected.

By investigating the dynamics of the field moment ratio R we can also determine relationships between important statistical quantities, such as the field correlation length ξ_e and the field localization length ξ_f. By the field correlation length ξ_e, we mean the average distance between the field peaks, while their spatial extension we characterize with the field localization length ξ_f [22]. For nonoverlapping peaks, one can find that $R=N/(N_eN_F)=(\xi_e/\xi_f)^d$, where $N=(l/a)^d=L^d$ is the total number of sites, and $N_e=(l/\xi_e)^d$ is the total number of the field peaks, each one occupying $N_F=(\xi_f/a)^d$ sites. In general, for $L\gg p^{-1/d}$, we expect R to be a function of p (but not of L) and κ; the same is true for the statistical length ξ_e. To determine this dependence we run calculations for two loss factors, $\kappa=0.1$ and $\kappa=0.01$. As illustrated in Fig. 4(b), for both cases, R can be approximated as

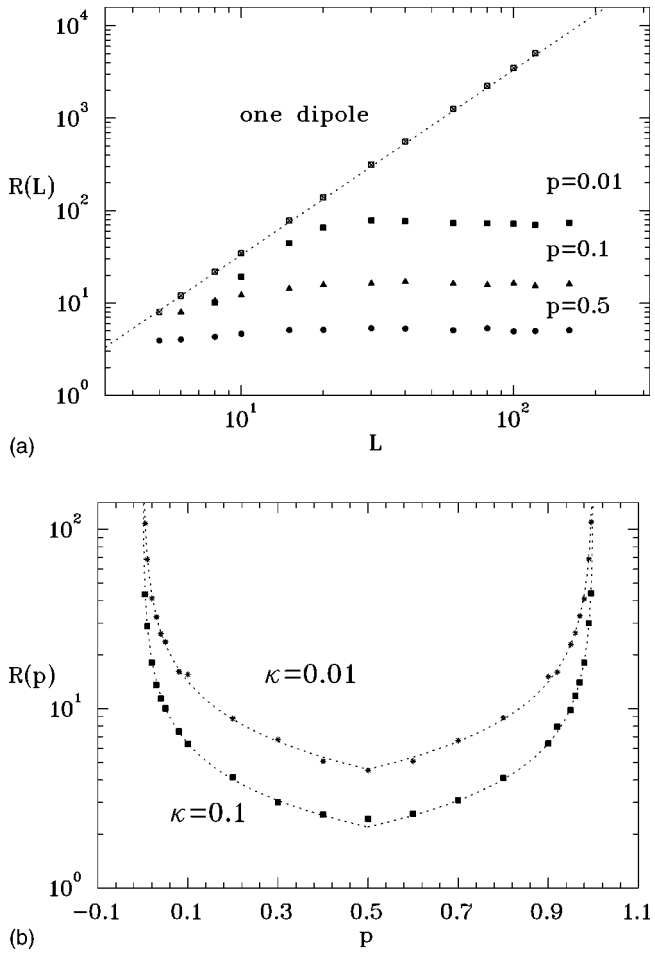

FIG. 4. The ratio of the local-field moments $R=M_4/(M_2)^2$. (a) R as a function of the lattice-size L (the crossed squares represent the data from BE calculations for a single dipole and the dashed line shows the analytical result). (b) R as a function of the metal filling factor p, for two different values of the loss factor κ (both values satisfy the inequality $\xi_e \ll aL$); the dashed lines represent a fit based on Eq. (13).

$$R(\kappa,p)=\eta(\kappa)\left\{\left[\theta(p)-\theta\left(p-\frac{1}{2}\right)\right]p^{-\tau} + \theta\left(p-\frac{1}{2}\right)(1-p)^{-\tau}\right\}, \tag{13}$$

where θ is the step function. For the exponent τ, we obtain a value which is close to 2/3. For $p \leqslant 0.5$ and $d=2$ this value yields the following relationship for the field correlation length: $\xi_e \simeq \xi_f p^{-1/3}\sqrt{\eta(\kappa)}=\xi_f(\xi_e/a)^{2/3}\sqrt{\eta(\kappa)}$, where the function $\eta(\kappa)$ increases when κ decreases. The analysis of the ratio ξ_e/ξ_f shows that we have a stronger localization with a decrease of both surface coverage p and loss factor κ. In the special case of a single dipole we have $R=(\xi_e/\xi_f)^2 = \frac{1}{3}L^2$, which, combined with $\xi_e=aL$, yields for the field localization length $\xi_f=a\sqrt{3}$.

The localization of the local fields into "hot" spots can be easily seen in Fig. 5, where we show (for different wavelengths) the spatial distribution for the local intensity $I(\mathbf{r})$,

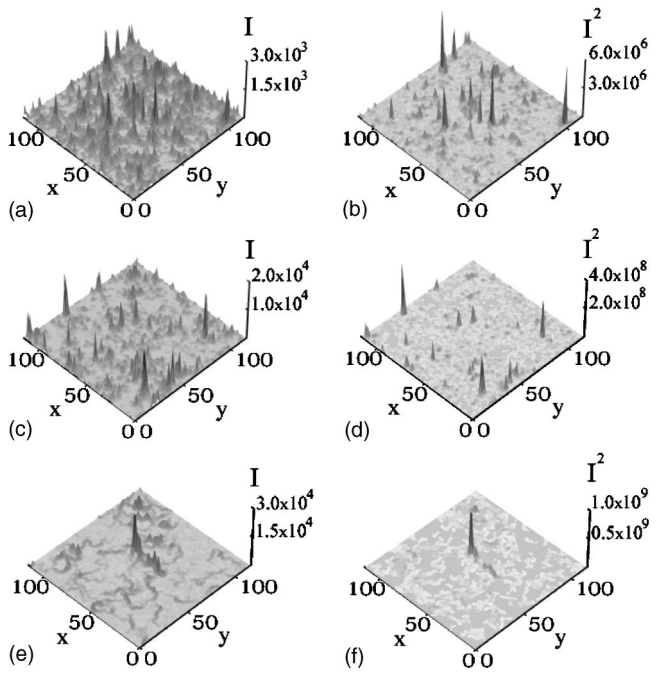

FIG. 5. The spatial distributions for the normalized local intensity $I(x,y)$ and for the "local Raman enhancement factor" $I^2(x,y)$. The distributions are calculated for three different wavelengths: $\lambda = 0.370$ μm (a),(b), $\lambda = 1$ μm (c),(d), and $\lambda = 5$ μm (e),(f). The metal filling factor is chosen as $p=p_c$, for all cases.

and for the fourth moment of the local fields $I^2(\mathbf{r})$. Note that $I^2(\mathbf{r})$ is proportional to the local Raman scattering enhancement provided that Raman-active molecules cover the film [7]. As mentioned, the resonance condition for isolated silver particles is satisfied at the wavelength $\lambda \approx 370$ nm. In Fig. 5, we see that the fluctuating local fields are well localized and enhanced with the enhancement on the order of 10^4 for $I(\mathbf{r})$ and 10^9 for $I^2(\mathbf{r})$. The spatial separation of the local peaks as well as their absolute magnitudes increase with the increase of λ. All these results qualitatively agree with the previously developed theory [4–8].

Based on the localization of plasmons, the scaling theory predicts that there should be a power-law dependence for the higher-order field moments

$$M_n=\langle|\mathbf{E}|^n\rangle/|\mathbf{E}_0|^n \sim \int \frac{\rho(\Lambda)[a/\xi_f(\Lambda)]^{2n-d}}{[\Lambda^2+\kappa^2]^{n/2}}d\Lambda \sim \kappa^{-n+1}, \tag{14}$$

where $n=2,3,4,\ldots$, $\rho(\Lambda)$ is the density of states, $\xi_f(\Lambda)$ represents the average single mode localization length which corresponds to eigenvalue Λ, and κ is the loss factor [7]. This functional dependence was checked earlier, using the approximate real space renormalization group method, where qualitative agreement was accomplished with Eq. (14). However, since the renormalization procedure is not exact, it is worth estimating the field moments with the exact BE method. To determine field moments M_n, we use the BE procedure for the surface filling fraction $p=p_c$ and a loss factor varying in the range $\kappa \in 1-10^{-3}$ ($\sigma_d=-i$, $\sigma_m=i$

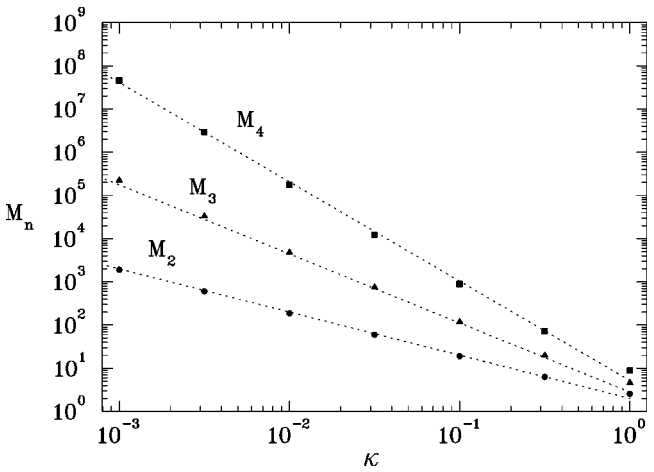

FIG. 6. High-order field moments M_2, M_3, and M_4, as functions of loss parameter κ; the calculations were performed for 100 different realizations in each case, for a lattice with size $L=120$.

$+\kappa$). All points are fitted with a power-law function, as shown in Fig. 6. For M_2 we obtained the exponent $x_2=1.0\pm0.1$, which is close to what was predicted by the scaling theory. For the third and fourth moments, we obtain that $M_{3,4}\sim\kappa^{-x_{3,4}}$, where the exponents $x_{3,4}$ are estimated as $x_3=1.7\pm0.1$ and $x_4=2.4\pm0.2$. These two exponents are somewhat different from the value predicted from Eq. (14): $x_3=2$ and $x_4=3$.

The scaling solution given by Eq. (14) is based on the assumption that the localization length $\xi_f(\Lambda)$ is finite for all Λ and it does not scale with the size of the system. If the function $\xi_f(\Lambda)$ has a pole, for example, at $\Lambda=0$ (note that in the previous publications, we used the notation ξ_A for this case), this can lead to a change in the scaling indices. The minimum of the correlation length ξ_e at the percolation threshold and the log-normal distribution resulting from the strong coupling between the dipoles also suggest that at $\Lambda=0$ we can expect the localization-delocalization transition [10,31]. To determine the function $\xi_f(\Lambda)$ we solve the eigenvalue problem for the real part $\hat{\mathbf{H}}'$ of the Kirchhoff's Hamiltonian $\hat{\mathbf{H}}=\hat{\mathbf{H}}'+i\kappa\hat{\mathbf{H}}''$ in 2D. The eigenvalue problem was solved with MATHEMATICA software for lattice sizes up to $L=50$. In our calculations of the localization length we used the inverse participation ratio so that for each eigenmode $\mathbf{\Psi}_n$ that satisfies the equation $\hat{\mathbf{H}}'\mathbf{\Psi}_n=\Lambda_n\mathbf{\Psi}_n$, the surface-averaged localization length for the nth mode $\xi_f^{(n)}$ is given by the relation $\xi_f^{(n)}=a\{[\Sigma_{i,j}^N|\mathbf{E}_n(i,j)|^4]/[\Sigma_{i,j}^N|\mathbf{E}_n(i,j)|^2]^2\}^{-1/d}$, where we have used the relationships $R_{IP}=R/L^d=(N_eN_f)^{-1}=(a/\xi_f)^d$ for $N_e=1$ (single mode) and $\mathbf{E}_n=-\boldsymbol{\nabla}\mathbf{\Psi}_n$. Results for the average localization length are shown in Fig. 7. This figure illustrates that all states but $\Lambda=0$ are localized as predicted by the theory. The localization lengths $\xi_f^{(n)}$ are symmetrically distributed with respect to the zero eigenvalue and scales as a power law $\xi_f(\Lambda)\sim\Lambda^{-\chi}$ (this is shown in the log-log inset). For the scaling exponent we obtain a value $\chi=0.14\pm0.02$ which leads to an improved relation for the field moments in the form $M_n\sim\kappa^{-n(1-\chi)+1}$. The exponents x_3 and x_4 are given now by $x_3=1.58\pm0.06$ and $x_4=2.44\pm0.08$, which is in good agreement with those found in the simulations. We note that, although the presence of delocalized states at $\Lambda=0$ results in a slight change of the critical exponents in Eq. (14), all basic conclusions of the previously developed scaling theory still hold because the relative weight of the delocalized states is small.

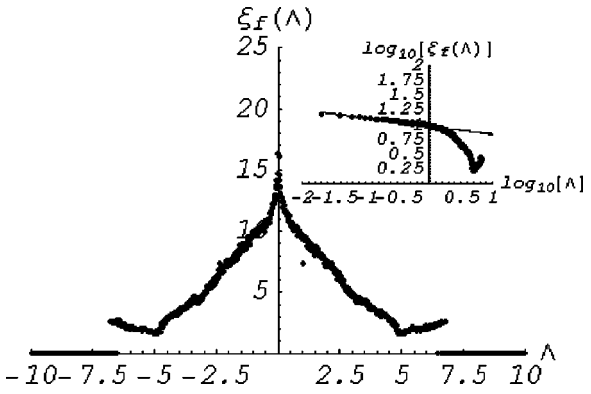

FIG. 7. Localization length $\xi_f(\Lambda)$ as a function of the eigenvalues Λ calculated for metal concentration equal to the percolation threshold p_c. The log-log inset depicts the scaling region with an exponent $\chi\approx0.14$.

The presence of nonlocalized states in random metal-dielectric films was also found in Ref. [10]. While our results are in qualitative agreement with [10], it is difficult to compare them quantitatively. This difficulty arises from the fact that in calculations of the localization length, the authors of [10] rely on the gyration radius. However, for eigenstates consisting of two (or more) spatially separated peaks, the gyration radius is characterized by the distance between the peaks rather than by the spatial sizes of individual peaks, which can be much smaller than the peak separation. In contrast, the inverse participation ratio used above characterizes the sizes of individual modes. We note that thus defined quantity ξ_f enters Eq. (14) and other formulas of the scaling theory.

VI. DISCUSSION AND CONCLUSIONS

In this paper we introduced a numerical method that we refer to as block elimination. The BE method takes advantage of the block structure of the Kirchhoff Hamiltonian $\hat{\mathbf{H}}$ and thus decreases the amount of numerical operations and memory required for solving the Kirchhoff equations for square networks. Note that the method is exact as opposed to previously used numerical methods, most of which are approximate. The results obtained show that the BE method reproduces well the known critical exponents and distribution functions obtained by other methods. The BE verifies the large enhancement of the local electric field predicted by the earlier theory [4–8]. Specifically, the BE results are in good accord with the estimates following from the real space renormalization group.

In addition to suggesting an efficient numerical method, we thoroughly examined the local-field distribution function

$P(I)$ for different metal filling factors p and loss factors κ. The important result here is that in the optical and infrared spectral range, the local electric field intensity is distributed over an exponentially broad range; specifically, the function $P(I)$ can be characterized by the log-normal function. The latter result, however, holds only in the close vicinity of the percolation threshold and for light frequencies close or equal to the surface plasmon resonance of individual metal particles. For metal concentrations far away from the percolation region, a power-law behavior was found for $P(I)$. This ''scaling'' tail in the local-field distribution can be related to the one-dipole distribution function. The BE method also verifies the localization of plasmons predicted earlier by the scaling theory. The ensemble average high-order moments for the local field have also been calculated. We found power-law exponents that are in qualitative accord with the scaling theory. With the introduction of corrections due to the presence of extended eigenmodes in the KH we obtained very good agreement between theory and simulations.

ACKNOWLEDGMENTS

This work was supported by Battelle under Contract No. DAAD19-02-D-0001, NASA (Contract No. NCC-1-01049), ARO (Contract No. DAAD19-01-1-0682), and NSF (Contract No. E SC-0210445).

APPENDIX

In this appendix we outline the construction of the KH in terms of the bond conductivities. As we show in Sec. II, the Kirchhoff equations in the quasistatic approximation provide solutions for the field distribution in a composite medium. We consider the construction of the matrix Eq. (4) for the two-dimensional case (the three-dimensional procedure is analogous) and treat a metal-dielectric film as a square lattice of size L. The field potentials in the sites of the lattice are described by the vector $\{\varphi_i\}$, where $i=1,2,\ldots,L^2$. All sites are connected by conducting bonds $\sigma_{i,j}$, where the index $j=\{i-1,i+1,i+L,i-L\}$ includes all the nearest neighbors for site i. Then we can rewrite Eq. (1) in the following form:

$$-\frac{1}{\Delta}[\sigma_{i,i+1}(\varphi_{i+1}-\varphi_i)-\sigma_{i,i-1}(\varphi_i-\varphi_{i-1})]+E_{0x}(\sigma_{i,i+1}-\sigma_{i,i-1})-\frac{1}{\Delta}[\sigma_{i,i+L}(\varphi_{i+L}-\varphi_i)-\sigma_{i,j-L}(\varphi_i-\varphi_{i-L})]+E_{0y}(\sigma_{i,i+L}-\sigma_{i,i-L})=0, \tag{A1}$$

where $\Delta=a=1/L$ is the bond length and the pair (E_{0x},E_{0y}) represents the components of the applied electric field. We can rewrite Eq. (A1) in a slightly different way:

$$h_{i,i}^{(jj)}\varphi_{i+(j-1)L}+h_{i,i+1}^{(jj)}\varphi_{i+(j-1)L+1}+h_{i,i-1}^{(jj)}\varphi_{i+(j-1)L-1}+h_{i,i}^{(j,j+1)}\varphi_{i+jL}+h_{i,i}^{(j-1,j)}\varphi_{i+(j-2)L}=F_i^{(j)}, \tag{A2}$$

where if $i'=i+(j-1)L$ and $L<i'<L^2-L$ the components of matrices $h^{(ij)}$ and vectors $F^{(j)}$ can be written as $h_{i,i}^{(jj)}=\sigma_{i',i'+1}+\sigma_{i',i'-1}+\sigma_{i',i'+L}+\sigma_{i',i'-L}$, $h_{i,i+1}^{(jj)}=-\sigma_{i',i'+1}$, $h_{i,i-1}^{(jj)}=-\sigma_{i',i'-1}$, $h_{i,i}^{(j,j+1)}=-\sigma_{i',i'+L}$, $h_{i,i}^{(j-1,j)}=-\sigma_{i',i'-L}$, and $F_i^{(j)}=-\Delta[E_{0x}(\sigma_{i',i'+1}-\sigma_{i',i'-1})+E_{0y}(\sigma_{i',i'+L}-\sigma_{i',i'-L})]$. The elements in the first and the last rows of matrix $\hat{\mathbf{H}}$ in Eq. (4), however, must be described in accordance with the boundary conditions. If the parallel boundaries (zero on the bottom and unity on the top) are used, then $h_{i,j}^{(11)}=h_{i,j}^{(LL)}=\delta_{ij}$; for the periodic boundary conditions, the matrix elements are described by relations similar to Eq. (3). As an example for the periodic boundary conditions, we show the exact forms of the 4×4 matrices $h^{(11)}$, $h^{(12)}$, and $h^{(15)}$:

$$h^{(11)}=\begin{pmatrix} \sigma_{1,4}+\sigma_{1,2}+\sigma_{1,13}+\sigma_{1,5} & -\sigma_{1,2} & 0 & -\sigma_{1,4} \\ -\sigma_{2,1} & \sigma_{2,3}+\sigma_{2,1}+\sigma_{2,14}+\sigma_{2,6} & -\sigma_{2,3} & 0 \\ 0 & -\sigma_{3,2} & \sigma_{3,4}+\sigma_{3,2}+\sigma_{3,15}+\sigma_{3,7} & -\sigma_{3,4} \\ -\sigma_{4,1} & 0 & -\sigma_{4,3} & \sigma_{4,1}+\sigma_{4,3}+\sigma_{4,16}+\sigma_{4,8} \end{pmatrix}, \tag{A3}$$

$$h^{(12)}=\begin{pmatrix} -\sigma_{1,5} & 0 & 0 & 0 \\ 0 & -\sigma_{2,6} & 0 & 0 \\ 0 & 0 & -\sigma_{3,7} & 0 \\ 0 & 0 & 0 & -\sigma_{4,8} \end{pmatrix}, \quad h^{(15)}=\begin{pmatrix} -\sigma_{1,13} & 0 & 0 & 0 \\ 0 & -\sigma_{2,14} & 0 & 0 \\ 0 & 0 & -\sigma_{3,15} & 0 \\ 0 & 0 & 0 & -\sigma_{4,16} \end{pmatrix}, \tag{A4}$$

where for the bond conductivities we have $\sigma_{i,j}=\sigma_{j,i}$. We should point out that for the periodic boundaries the matrix $\hat{\mathbf{H}}$ has rank L^2-1, and in order for the system to have a solution, one of the site potentials must be grounded.

[1] W. L. Mochan and R. G. Barrera, Physica A **241**, 1 (1997).
[2] D. J. Bergman and D. Stroud, Solid State Phys. **46**, 147 (1992).
[3] A. K. Sarychev, Zh. Eksp. Teor. Fiz. **72**, 1001 (1977).
[4] V. M. Shalaev and A. K. Sarychev, Phys. Rev. B **57**, 13 265 (1998).
[5] A. K. Sarychev, V. A. Shubin, and V. M. Shalaev, Phys. Rev. B **60**, 16 389 (1999).
[6] A. K. Sarychev, V. A. Shubin, and V. M. Shalaev, Phys. Rev. E **59**, 7239 (1999).
[7] A. K. Sarychev and V. M. Shalaev, Phys. Rep. **335**, 275 (2000).
[8] V. M. Shalaev, *Nonlinear Optics of Random Media: Fractal Composites and Metal-Dielectric Films*, Springer Tracts in Modern Physics Vol. 158 (Springer, Berlin, 2000).
[9] S. Gresillon, L. Aigouy, A. C. Boccara, J. C. Rivoal, X. Quelin, C. Desmarest, P. Gadenne, V. A. Shubin, A. K. Sarychev, and V. M. Shalaev, Phys. Rev. Lett. **82**, 4520 (1999).
[10] M. I. Stockman, S. V. Faleev, and D. J. Bergman, Phys. Rev. Lett. **87**, 167401 (2001).
[11] D. J. Frank and C. J. Lobb, Phys. Rev. B **37**, 302 (1988).
[12] L. Tortet, J. R. Gavarri, J. Musso, G. Nihoul, J. P. Clerc, A. N. Lagarkov, and A. K. Sarychev, Phys. Rev. B **58**, 5390 (1998).
[13] A. K. Sarychev and A. P. Vinogradov, J. Phys. C **14**, L487 (1981).
[14] J. P. Clerc, V. A. Podolskiy, and A. K. Sarychev, Eur. Phys. J. B **15**, 507 (2000).
[15] B. Derrida and J. Vannimenus, J. Phys. A **15**, L557 (1982).
[16] S. Kirkpatrick, Phys. Rev. Lett. **27**, 1722 (1971).
[17] G. G. Bartrouni, A. Hansen, and M. Nelkin, Phys. Rev. Lett. **57**, 1336 (1986).
[18] L. Zekri, R. Bouamrane, and N. Zekri, J. Phys. A **33**, 649 (2000).
[19] R. Coult *et al.*, *Computational Methods in Linear Algebra* (Wiley, New York, 1975).
[20] V. Privman, *Finite-Size Scaling and Numerical Simulations of Statistical System* (World Scientific, Singapore, 1988).
[21] D. Stauffer and A. Aharony, *Introduction to Percolation Theory*, 2nd ed. (Taylor and Francis, London, 1992).
[22] F. Brouers, S. Blacher, and A. K. Sarychev, Phys. Rev. B **58**, 15 897 (1998).
[23] J. Cardy, *Finite-Size Scaling* (North-Holland, Amsterdam, 1981).
[24] A. Aharony, R. Blumenfeld, and A. B. Harris, Phys. Rev. B **47**, 5756 (1993).
[25] L. Zekri, R. Bouamrane, N. Zekri, and F. Brouers, J. Phys.: Condens. Matter **12**, 283 (2000).
[26] *Handbook of Optical Constants of Solids*, edited by E. D. Palik (Academic Press, New York, 1985).
[27] M. I. Stockman, L. N. Pandey, L. S. Muratov, and T. F. George, Phys. Rev. Lett. **72**, 2486 (1994).
[28] S. Bozhevolnyi and V. Coello, Phys. Rev. B **64**, 115414 (2001).
[29] Katayayani Seal, M. A. Nelson, Z. C. Ying, D. A. Genov, A. K. Sarychev, and V. M. Shalaev, Phys. Rev. B **67**, 035318 (2003).
[30] B. Kramer and A. MacKinnon, Rep. Prog. Phys. **56**, 1469 (1993).
[31] K. Muller, B. Mehlig, F. Milde, and M. Schreiber, Phys. Rev. Lett. **78**, 215 (1997).